

IMAGING A CENTRAL IONIZED COMPONENT, A NARROW RING, AND THE CO SNOWLINE IN THE MULTI-GAPPED DISK OF HD 169142

ENRIQUE MACÍAS

Department of Astronomy, Boston University, 725 Commonwealth Avenue, Boston, MA 02215, USA
 Instituto de Astrofísica de Andalucía (CSIC) Glorieta de la Astronomía s/n E-18008 Granada, Spain emacias@bu.edu

GUILLEM ANGLADA, MAYRA OSORIO

Instituto de Astrofísica de Andalucía (CSIC) Glorieta de la Astronomía s/n E-18008 Granada, Spain

JOSÉ M. TORRELLES

Institut de Ciències de l'Espai (CSIC) and Institut de Ciències del Cosmos (UB)/IEEC, Can Magrans S/N, Cerdanyola del Vallès (Barcelona), Spain

CARLOS CARRASCO-GONZÁLEZ

Instituto de Radioastronomía y Astrofísica UNAM, Apartado Postal 3-72 (Xangari), 58089 Morelia, Michoacán, Mexico

JOSÉ F. GÓMEZ

Instituto de Astrofísica de Andalucía (CSIC) Glorieta de la Astronomía s/n E-18008 Granada, Spain

LUIS F. RODRÍGUEZ & ANIBAL SIERRA

Instituto de Radioastronomía y Astrofísica UNAM, Apartado Postal 3-72 (Xangari), 58089 Morelia, Michoacán, Mexico

ABSTRACT

We report Very Large Array observations at 7 mm, 9 mm, and 3 cm toward the pre-transitional disk of the Herbig Ae star HD 169142. These observations have allowed us to study the mm emission of this disk with the highest angular resolution so far ($0''.12 \times 0''.09$, or $14 \text{ au} \times 11 \text{ au}$, at 7 mm). Our 7 and 9 mm images show a narrow ring of emission at a radius of $\sim 25 \text{ au}$ tracing the outer edge of the inner gap. This ring presents an asymmetric morphology that could be produced by dynamical interactions between the disk and forming planets. Additionally, the azimuthally averaged radial intensity profiles of the 7 and 9 mm images confirm the presence of the previously reported gap at $\sim 45 \text{ au}$, and reveal a new gap at $\sim 85 \text{ au}$. We analyzed archival DCO⁺(3-2) and C¹⁸O(2-1) ALMA observations, showing that the CO snowline is located very close to this third outer gap. This suggests that growth and accumulation of large dust grains close to the CO snowline could be the mechanism responsible for this proposed outer gap. Finally, a compact source of emission is detected at 7 mm, 9 mm, and 3 cm toward the center of the disk. Its flux density and spectral index indicate that it is dominated by free-free emission from ionized gas, which could be associated with either the photoionization of the inner disk, an independent object, or an ionized jet.

Keywords: ISM: jets and outflows — protoplanetary disks — planet-disk interactions — stars: individual (HD 169142) — stars: pre-main sequence

1. INTRODUCTION

Planetary systems are formed in circumstellar disks around pre-main sequence stars. Tidal interactions be-

tween the forming planets and the disk can result in complex substructures such as cavities, gaps, spirals, or lopsided rings ([Baruteau et al. 2014](#)). Studying disks

showing these features could provide us with critical information about the planetary formation process itself. In particular, transitional disks, which are protoplanetary disks with central dust gaps or cavities typically of tens of au in size (Strom et al. 1989), appear as excellent candidates to study the first stages of planetary formation.

Cavities in transitional disks were first identified through modeling of their spectral energy distributions (SEDs) (Calvet et al. 2005). This modeling also led to the discovery of a subfamily of transitional disks, the so-called pre-transitional disks, which are thought to present a residual inner disk inside the cavity that can still emit significantly at near-IR wavelengths (Espaillet et al. 2007). (Sub-)mm and polarimetric IR observations have been able to image several of these disks and confirm the presence of the central cavities or gaps (e.g., Andrews et al. 2011; Quanz et al. 2011). Since their discovery, a number of mechanisms have been proposed to explain these inner clearings of dust (Espaillet et al. 2014 and references therein). Nevertheless, observations seem to indicate that most cavities in transitional disks are created by dynamical interactions with orbiting sub-stellar or planetary companions (Andrews et al. 2011; Espaillet et al. 2014).

Until recent years, (sub-)mm observations lacked the sensitivity and angular resolution necessary to reach distances very close to the central star. With the outstanding angular resolution provided by the most extended baselines of the Atacama Large Millimeter/Submillimeter Array (ALMA), as well as with the new capabilities of the Karl G. Jansky Very Large Array (VLA), it is now possible to attempt this type of studies. In particular, recent ALMA observations have revealed the presence of very small central cavities, few au in size, in some transitional disks (e.g., XZ Tau B: Osorio et al. 2016; TW Hya: Andrews et al. 2016). On the other hand, in a few cases it has been possible to detect compact central emission inside the cavity of transitional disks (Isella et al. 2014; Rodríguez et al. 2014; Andrews et al. 2016). This central emission has been associated with an inner disk (emission either from dust or from photoionized gas) or with an ionized jet.

Additionally, (sub-)mm ALMA observations have also revealed the presence of several gaps and rings up to distances of ~ 90 au from the star in the protoplanetary disk around HL Tau (ALMA Partnership et al. 2015). These gaps, however, might have a different origin to those observed at the inner regions of transitional disks. The young age of HL Tau, as well as the fact that some gaps are very narrow and appear at very long distances from the star, have led to question whether a planet could produce this type of gaps. This has resulted in a number of studies proposing new physical processes

that could create similar gap structures – e.g. zonal flows in magnetized disks (Bai & Stone 2014), magneto-rotational instability at the dead zone outer edge (Flock et al. 2015), sintering-induced gaps and rings (Okuzumi et al. 2016), or grain growth close to snowlines in the disk (Ros & Johansen 2013; Zhang et al. 2015). Gaps produced by these mechanisms could also be present in older protoplanetary and transitional disks, but they would have remained unnoticed in previous (sub-)mm observations due to a lack of sensitivity and angular resolution. In fact, recent ALMA observations, with a similar angular resolution to the HL Tau observations, have revealed the presence of similar ringed substructures in the transitional disk of TW Hya (Andrews et al. 2016) and in the protoplanetary disk of HD 163296 (Isella et al. 2016). Similar observations of protoplanetary disks at these high angular resolutions could show whether multi-gap structures are ubiquitous in protoplanetary disks, and will help to identify the physical mechanisms responsible for their creation.

HD 169142 is a Herbig Ae star ($M_{\star} \simeq 1.65\text{--}2 M_{\odot}$, age $\simeq 5\text{--}11$ Myr, Blondel & Djie 2006; Manoj et al. 2006) surrounded by an almost face-on ($i \simeq 13^{\circ}$; Raman et al. 2006) pre-transitional disk (Osorio et al. 2014 and references therein). Osorio et al. (2014) presented VLA observations at 7 mm toward HD 169142, detecting a bright ring of dust emission at a radius of $\sim 0''.2$ surrounding a central cavity, as well as an outer gap from $\sim 0''.28$ to $\sim 0''.48$, coincident with the results from IR polarized scattered light images (Quanz et al. 2013; Momose et al. 2015; Monnier et al. 2017). These results have been confirmed by recent ALMA 1.3 mm continuum and CO observations, showing that the two dust gaps are filled in with gas with a significantly reduced density at radii smaller than $\sim 0''.48$ (Fedele et al. 2017). The 7 mm emission ring imaged by Osorio et al. (2014) shows an azimuthally asymmetric morphology, reminiscent of the lopsided morphology produced as a consequence of dust trapping in planet-induced vortices (Birnstiel et al. 2013). These authors also reproduced the SED and 7 mm radial intensity profile of HD 169142 with a disk model that included the central cavity and the outer gap. Their results show that an inner residual disk is required to fit the SED and concluded that the disk of HD 169142 is a pre-transitional disk with two gaps. Their results also suggested that planet formation is the most likely origin for both detected gaps. In fact, a substellar or planetary companion candidate has been detected within the inner gap of the disk (Reggiani et al. 2014; Biller et al. 2014), which supports a planet-induced origin for this gap.

We note that most of the previous studies of HD 169142 adopted a distance of 145 pc (van Boekel et al. 2005). However, the recent publication of the first data

release of Gaia has revealed that the distance to HD 169142 is 117 ± 4 pc (Gaia Collaboration et al. 2016). This represents a decrease of $\sim 20\%$ from the value of 145 pc adopted in the literature. The same reduction has been therefore applied throughout this article to the sizes of the disk structures measured here and in the literature.

In this paper we present new high angular resolution VLA observations at 7 mm, 9 mm, and 3 cm toward the pre-transitional disk around HD 169142, revealing the presence of a new third gap in the disk as well as a free-free thermal emission source inside the inner gap.

2. OBSERVATIONS

We performed observations using the VLA of the National Radio Astronomy Observatory (NRAO)¹ in the A and BnA configurations at Q (~ 7 mm), Ka (~ 9 mm), and X (~ 3 cm) bands. Archival observations at K (~ 1.3 cm; C and DnC configurations) and C bands (~ 5 cm; A configuration) were also used (see Table 1). Amplitude calibration was performed by observing 3C286, with an expected uncertainty in the flux scale of $\sim 10\%$. 3C286 was also used as the bandpass and delay calibrator, whereas J1820-2528 was used as the complex gain calibrator.

Table 1. VLA observations

Band	Central Frequency (GHz)	Bandwidth (GHz)	Array Configuration	Observation Date	Project Code	On-source time (min)
Q	44	8	A	2014-Mar-06	14A-496	63.9
				2014-Mar-04		63.9
				2014-Feb-27		63.9
Q	44	8	BnA	2014-Jan-25	13B-260	72.0
Q	44	8	B	2013-Sep-28 ^a	13B-260	72.0
Ka	33	8	A	2014-Feb-25	14A-496	45.4
K	21	2	C	2012-Jan-29	AC982	6.0
			DnC	2010-Sep-30		6.0
X	10	4	A	2014-Mar-06	14A-496	15.3
				2014-Mar-04		15.3
				2014-Feb-27		46.0
				2014-Feb-25		15.3
X	9	2	BnA	2014-Jan-25	13B-260	7.3
X	9	2	B	2013-Sep-28 ^a	13B-260	7.3
C	5.5	2	A	2012-Dec-23	12A-439	8.0
				2012-Nov-12 ^a		8.0

^a Data reported in Osorio et al. (2014).

The observations were reduced and calibrated with the reduction package Common Astronomy Software Applications (CASA; version 4.5.3; McMullin et al. 2007)². Each data set was processed through the VLA calibra-

tion pipeline integrated within CASA. After each run of the pipeline the calibrated data were inspected. Then, we performed additional data flagging and re-ran the pipeline as many times as needed.

Deconvolved images were produced with the CLEAN task of CASA. A multi-scale multi-frequency deconvolution algorithm was used to take into account the frequency dependence of the emission within each band (Rau & Cornwell 2011). Data from each observing session were first imaged independently to check for possi-

¹ The NRAO is a facility of the National Science Foundation operated under cooperative agreement by Associated Universities, Inc.

² <https://science.nrao.edu/facilities/vla/data-processing>

ble errors in the absolute position, without finding any significant shift. Then, for each band, we combined the data from the different epochs and configurations in order to obtain higher sensitivity images. A *uvtaper* was applied to the Ka band visibilities in order to improve the signal to noise ratio of the image.

In addition, we report unpublished archival Atacama Large Millimeter/submillimeter Array (ALMA) data of the $\text{DCO}^+(3-2)$ transition (rest frequency 216.112 GHz), and we reanalyze data of the $\text{C}^{18}\text{O}(2-1)$ transition (rest frequency 219.560 GHz). The observations were carried out on 2015 August 30 (project code: 2013.1.00592.S) and are described in Fedele et al. (2017), where the $\text{C}^{18}\text{O}(2-1)$ data were first reported. Data calibration was performed using the ALMA pipeline within CASA (version 4.3.1). Deconvolved images were then obtained using the CLEAN task with natural weighting. In addition, a *uvtaper* was applied to the $\text{DCO}^+(3-2)$ visibilities in order to achieve a higher signal-to-noise ratio. The rms noise of the $\text{C}^{18}\text{O}(2-1)$ observations is ~ 6 mJy beam $^{-1}$ (synthesized beam of $0''.35 \times 0''.23$, PA= -74°) for a channel width of ~ 0.25 km s $^{-1}$, whereas the rms noise of the $\text{DCO}^+(3-2)$ observations is ~ 7 mJy beam $^{-1}$ (synthesized beam of $0''.50 \times 0''.48$, PA= -65°) for a channel width of ~ 0.25 km s $^{-1}$.

3. RESULTS AND DISCUSSION

A natural-weighted image of the 7 mm emission of HD 169142, obtained from the combination of A, BnA, and B configuration data, is shown in Figure 1. The image shows a narrow ring of emission of radius $\sim 0''.21$ (~ 25 au at 117 pc) with significant substructure. In addition, the image shows a hint of a second ring of emission at $\sim 0''.50$ (~ 59 au) tracing the rim of the second gap detected by Osorio et al. (2014). A compact emission component is detected inside the inner ring, with its peak of emission displaced a projected distance of $\sim 0''.023$ (~ 2.7 au) from its center. In the images made from a single configuration, this central component of emission is only detected in the A configuration data, which have enough angular resolution and sensitivity to separate it from the ring of emission. We do not expect significant proper motions within the time span of the A configuration observations (one week). Thus, we expect that our images obtained combining the A, BnA, and B configuration data will not be affected by these proper motions. The total flux density of the 7 mm emission is 2.0 ± 0.4 mJy, which is consistent with previous measurements (Osorio et al. 2014). The flux density of the central component is 74 ± 15 μ Jy.

Our new A configuration data, with higher sensitivity and angular resolution, do not confirm the knot of 7 mm emission located $\sim 0.34''$ (~ 40 au) to the south of the central position, suggestive of a protoplanet can-

didate inside the second gap, that was observed in the Osorio et al. (2014) images. Also, we do not identify radio emission associated with the IR source detected by Reggiani et al. (2014) and Biller et al. (2014) at radius $0''.16$ and PA = 7° .

The left panel in Figure 2 presents the 9 mm image of HD 169142. This image shows a similar morphology to the 7 mm image: a ring of emission with a central radio source inside its cavity. The ring of emission also seems to show some substructure, although the low signal to noise ratio makes it difficult to determine whether this substructure in the 9 mm image is real or due to rms fluctuations. The total flux density of the 9 mm emission is 850 ± 150 μ Jy, while the flux density of the central emission inside the inner ring is 45 ± 14 μ Jy.

The right panel in Figure 2 shows an image of the 3 cm emission of HD 169142, obtained by combining the A, BnA, and B configuration observations using natural weighting. The emission is only marginally resolved, with its peak of emission located inside the inner dust gap, very close to the central star. The total flux density at 3 cm is 50 ± 10 μ Jy. Due to the lower angular resolution of the 3 cm observations, we cannot directly separate in our natural-weighted image the emission of the extended disk from the central radio source. By using a higher weight for the most extended visibilities, we can filter out the extended disk emission and estimate the flux density of the compact central radio source. We used Briggs weighting with a robust parameter of 0.5 (as defined in task CLEAN of CASA) and estimated a flux density at 3 cm of $\sim 20 \pm 5$ μ Jy for the central radio source. The remaining emission in the natural-weighted image at 3 cm is consistent with the dust flux density of ~ 30 μ Jy predicted by the model of Osorio et al. (2014).

Finally, no emission was detected in the K and C band observations, with 3σ upper limits of 420 μ Jy beam $^{-1}$ and 27 μ Jy beam $^{-1}$, respectively. The C band image was obtained by combining our new data with those previously reported by Osorio et al. (2014) in order to obtain a tighter upper limit. Both limits are consistent with the model presented by Osorio et al. (2014).

3.1. Narrow ring

As can be seen in Figure 1, our 7 mm image shows a narrow ring of emission with a radius of ~ 25 au. For the width of the ring we estimate a deconvolved FWHM of ~ 8 au, measured along the E-W direction, where the synthesized beam size is smaller. The ring in our images coincides quite well with the ring imaged in previous near-IR (Quanz et al. 2013; Monnier et al. 2017), 7 mm (Osorio et al. 2014), and 1.3 mm (Fedele et al. 2017) observations, but our images reveal additional details.

We have estimated the position of the center of the ring by fitting an ellipse with its major axis along

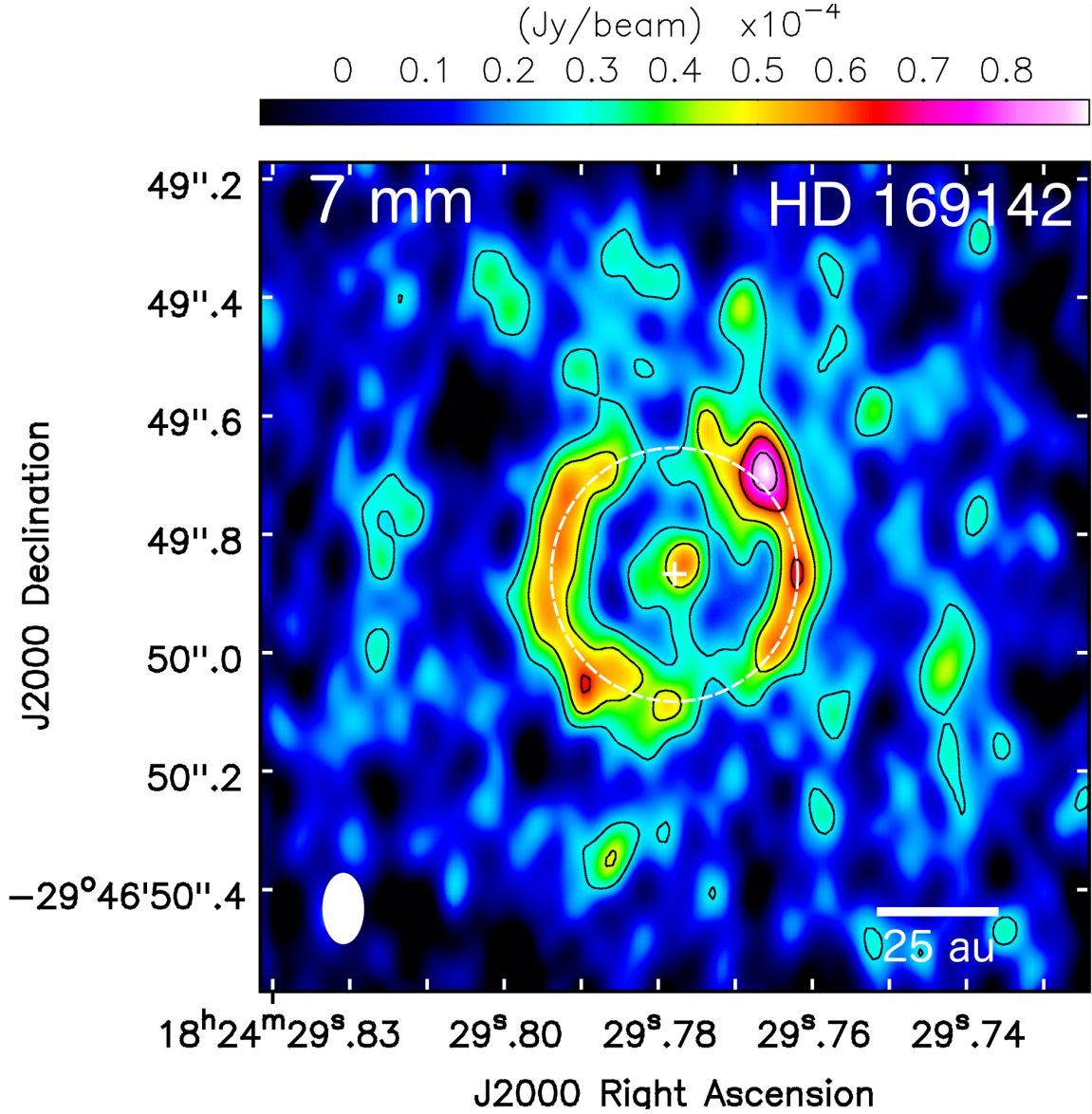


Figure 1. Natural-weighted VLA image at 7 mm of the transitional disk around HD 169142 (synthesized beam= $0''.12 \times 0''.07$, PA= 0° ; shown in the lower-left corner). Contour levels are $-3, 3, 5, 7$, and 9 times the rms of the map, $9.0 \mu\text{Jy beam}^{-1}$. The dashed ellipse indicates our fit to the ring image at 7 mm. The white cross shows the position of the center of the ring.

the position angle of the disk, as estimated from previous molecular observations (PA= 5° ; [Raman et al. 2006](#)), to the ring image, excluding the regions where two dips and a knot of emission are found (see below). From this fit we estimate that the center of the ring in the 7 mm image (epoch ~ 2014.17) is located at $\alpha(\text{J2000}) = 18^{\text{h}}24^{\text{m}}29^{\text{s}}.77798 \pm 0^{\text{s}}.00018$, $\delta(\text{J2000}) = -29^\circ46'49''.8673 \pm 0''.0028$, which coincides within $\sim 4 \pm 3$ mas with the position of the star HD 169142 given in the Gaia catalog, after correcting for proper motions ([Gaia Collaboration et al. 2016](#)). This result indicates that the ring is very well centered on the star, and that the alignment of the data to make the final image, as well as the quality of its astrometry, are very good. From our fit we also estimate a radius of the ring of $0''.214 \pm 0''.004$

(25.0 ± 0.5 au), which is slightly larger than the radius of $\sim 0''.19$ (~ 22 au) estimated from the near-IR scattered light images ([Quanz et al. 2013](#)). This suggests that the scattered light emission arises mainly from the inner rim or wall of the ring, whereas the 7 mm emission traces mainly the surface density of the large dust grains that peaks at slightly larger radii.

The intensity of the ring in our 7 mm image is significantly asymmetric in azimuth, showing a knot of emission $\sim 4 \sigma$ above the average intensity of the ring at PA $\simeq -40^\circ$, in agreement with the previous results of [Osorio et al. \(2014\)](#), who noted this azimuthal asymmetry from 7 mm data of lower angular resolution. We think that this knot represents a real azimuthal asymmetry since an intensity enhancement appears both in

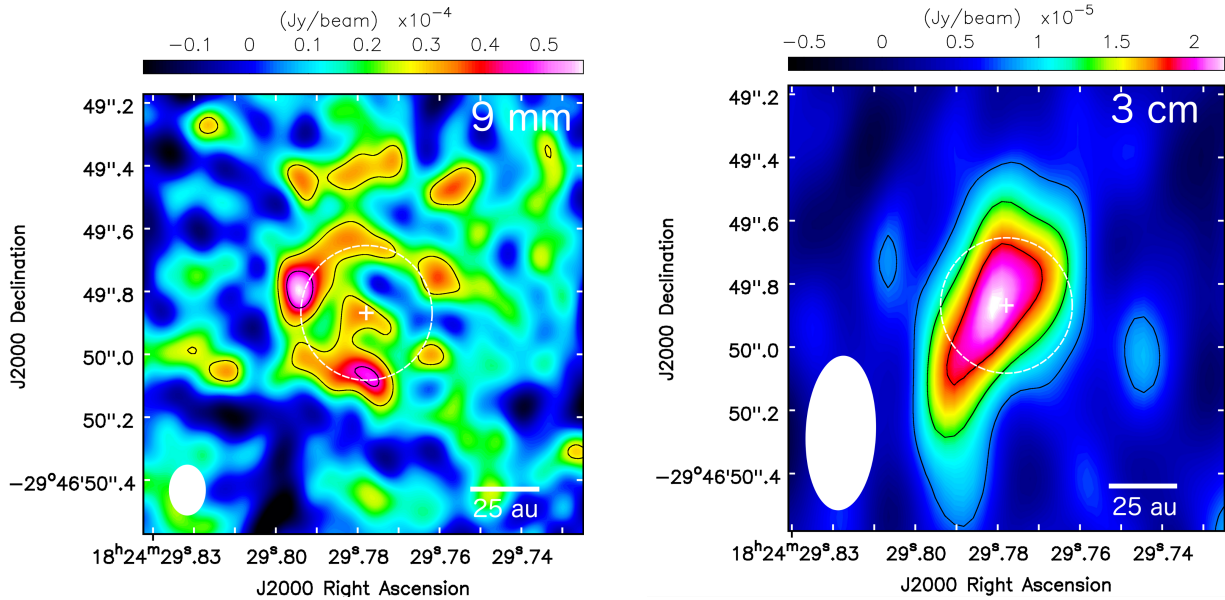


Figure 2. Left panel: Natural-weighted VLA image of the 9 mm emission (synthesized beam= $0''.16 \times 0''.12$, PA= 0° ; shown in the lower-left corner). Contour levels are $-3, 3, 5$, and 7 times the rms of the map, $9.0 \mu\text{Jy beam}^{-1}$. Right panel: Natural-weighted VLA image of the 3 cm emission (synthesized beam= $0''.49 \times 0''.22$, PA= -2.5° ; shown in the lower-left corner). Contour levels are $-3, 3, 5$, and 7 times the rms of the map, $2.6 \mu\text{Jy beam}^{-1}$. In both panels the dashed ellipse indicates our fit to the ring at 7 mm as shown in Figure 1. The white cross shows the position of the center of the ring.

the images made from the new A configuration data alone as well as in the lower angular resolution maps reported in [Osorio et al. \(2014\)](#). The ALMA 1.3 mm images also show a hint of this asymmetry ([Fedele et al. 2017](#)), although at a lower significance, probably due to the higher optical depth of the ring at shorter wavelengths, or an accumulation of the large dust grains preferentially traced at 7 mm.

On the other hand, our new 7 mm image also shows significant decreases of intensity or dips in the ring at PA $\simeq 0^\circ$ and PA $\simeq -170^\circ$. As shown by [Osorio et al. \(2014\)](#), an elongated beam can produce depressions of emission along the direction of the major axis of the beam in an axisymmetric ring. Additionally, noise fluctuations can produce spurious clumpy structures during the deconvolution process. In order to check whether the substructure detected in our images is real or due to these spurious effects, we obtained simulated images with random thermal noise using the model presented by [Osorio et al. \(2014\)](#) and the SIMOBSERVE task in CASA. These simulations showed that, for certain noise structures, intensity depressions similar to the ones in our observations could be formed in the narrow ring, suggesting that the observed dips in our 7 mm observations could be produced because of the combined effect of noise fluctuations and the elongated beam. Nevertheless, none of our simulations produced a bright knot similar to the one detected in our 7 mm observations, indicating that it is tracing a real azimuthal asymmetry in the ring.

Polarized scattered light images at H band show an axisymmetric ring with only a possible dip at a PA $\simeq 80^\circ$ ([Quanz et al. 2013](#)), where no significant drop of emission is seen in our images. The fact that the knot of emission in the ring is not present at near-IR wavelengths indicates that it is probably produced by azimuthal asymmetries in the density near the disk mid-plane, to which our 7 mm images are more sensitive, without affecting significantly the distribution of small dust grains in the disk atmosphere, which are traced by the scattered light images.

Azimuthal asymmetries in the large dust grains distribution are expected to be produced by tidal interactions between a forming planet and the disk (e.g., [Baruteau et al. 2014](#)). Hydrodynamic simulations show that planets can create relatively large cavities with vortices at their outer edges. These vortices, in turn, are able to trap the large dust grains in their pressure maxima, producing lopsided asymmetries at mm wavelengths ([Birnstiel et al. 2013](#); [Zhu & Stone 2014](#)). Thus, the interaction between the disk of HD 169142 and the possible forming planets at the inner ([Reggiani et al. 2014](#); [Biller et al. 2014](#)) and second gaps could be responsible for the observed non-axisymmetric structure.

3.2. Central compact radio source

Our 7 mm, 9 mm, and 3 cm images have revealed the presence of compact emission inside the bright emission ring, originating near its center (Figs. 1 and 2). The emission at 7 mm is slightly extended along the E-W

direction, with its intensity peak at a projected distance of $\sim 3 \pm 1$ au ($\sim 0''.025 \pm 0''.010$) from the central star toward the W direction. The quoted uncertainty is probably only a lower limit, corresponding to the formal error in the position of the emission peak relative to the center of the ring, estimated as $\sim 0.5(\theta/\text{SNR})$ (Reid et al. 1988), assuming an unresolved source ($\theta = 0''.1$) and a signal-to-noise ratio (SNR) of 5. Further observations are needed to confirm the reality and origin of this possible displacement (see below).

The insufficient sensitivity and angular resolution of the images at 9 mm and 3 cm, respectively, make it difficult to estimate the morphology of the central emission observed at these wavelengths. This central radio source could not be detected in previous observations by Osorio et al. (2014) toward HD 169142 at 7 mm due to the lack of angular resolution. We do not identify radio emission associated with the IR source detected by Biller et al. (2014) and Reggiani et al. (2014) located $\sim 0.16''$ (~ 19 au) north from the central star.

In principle, both dust and ionized gas could be contributing to the radio emission at the innermost regions of transitional disks. To our knowledge, very few transitional disks have been observed with high enough angular resolution to detect and resolve compact emission at mm and cm wavelengths inside their central cavities or gaps. LkCa 15 (Isella et al. 2014) and AB Aur (Rodríguez et al. 2014) were imaged with the VLA at 7 mm and 3 cm, respectively, whereas TW Hya was observed with ALMA at 0.87 mm (Andrews et al. 2016). The emission in TW Hya has been attributed to inner residual dust located close to the star, although it has also been recently suggested that a contribution of free-free emission from photoionized gas could be present (Ercolano et al. 2017). The morphology and spectral index of the emission in AB Aur indicates that it is associated with free-free emission from an accretion-driven jet. In LkCa 15, however, the lack of observations at other wavelengths makes it impossible to distinguish between a dust or a free-free origin for the emission. In the following we discuss the origin of the observed compact central radio source in HD 169142.

The near-IR excess in the SED of HD 169142 indicates that its disk is a pre-transitional disk, with a hot dust component located very close to the star. Osorio et al. (2014) modeled the broadband SED as well as the 7 mm images of HD 169142 and found that an inner disk of 0.6 au in radius, together with its inner wall at the dust sublimation radius (~ 0.2 au), could fit the near-IR emission of HD 169142. According to their model, this inner dust component would produce only $\sim 9 \mu\text{Jy}$, $\sim 5 \mu\text{Jy}$ and $< 1 \mu\text{Jy}$ of emission at 7 mm, 9 mm, and 3 cm, respectively. These values are much lower than the observed $74 \pm 15 \mu\text{Jy}$, $45 \pm 14 \mu\text{Jy}$ and $\sim 20 \pm 5 \mu\text{Jy}$ at

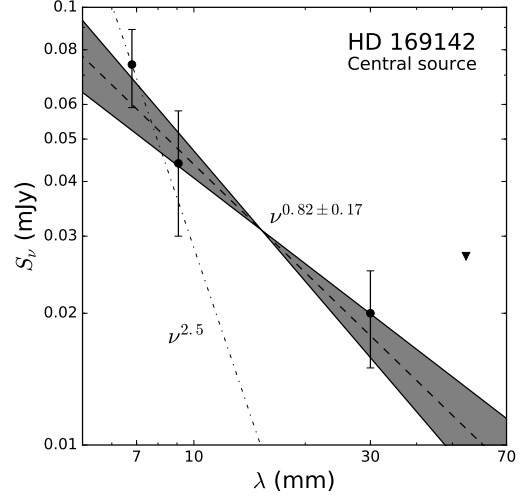


Figure 3. Spectral energy distribution of the radio emission of the central compact radio source in HD 169142. The black points and error bars represent our measured 7 mm, 9 mm, and 3 cm flux densities. The dashed black line indicates the power-law fit to these data. The grey area represents the uncertainty (1σ) of the fit. The dot-dashed line shows, as a reference, a power-law with a spectral index of 2.5, typical of dust thermal emission. The triangle indicates the non-detection upper limit for the flux density at 5 cm (C band).

these wavelengths for the central radio source. From a power-law fit to these observed values of the flux density ($S_\nu \propto \nu^\alpha$), we estimate a spectral index $\alpha = 0.82 \pm 0.17$ (see Fig. 3), which is too low to correspond to dust thermal emission (dust thermal emission presents $\alpha \geq 2$). Therefore, both the flux density and spectral index of the central radio source indicate that its emission is mainly dominated by partially optically-thick free-free emission from ionized gas.

Gas near young stellar objects has been found to be ionized by two main mechanisms: shocks in accretion-driven jets (Anglada et al. 2015), and photoionization due to the high energy radiation from the central star (Alexander et al. 2014). Since accretion and ejection of material are correlated (Cabrit 2007), low mass-accretion rate objects, such as transitional disks, are expected to present relatively weak radio jets. However, recent studies with the VLA have shown that radio jets in this type of sources can produce free-free emission at levels that are detectable with the improved sensitivity of the VLA (Rodríguez et al. 2014). In particular, Macías et al. (2016) presented VLA observations at 3 cm toward the transitional disk of GM Aur revealing resolved free-free emission from a radio jet and from a photoevaporating disk, showing that both mechanisms can contribute at the same level to the total free-free emission.

The central radio source detected at 7 mm in HD 169142 presents a slight elongation with a $\text{PA} \simeq -80^\circ$,

which is consistent with the position angle of the disk rotation axis ($PA \simeq -85^\circ$), as shown by molecular line observations (Raman et al. 2006). This suggests that the central radio source in our images could be tracing an accretion-driven radio jet. We can obtain a rough estimate of the free-free emission of an accretion-driven jet in HD 169142 with the empirical correlation between the radio luminosity of a source, $S_\nu d^2$, and its outflow momentum rate, \dot{P}_{out} (Anglada 1995; Anglada et al. 2015): $(\dot{P}_{\text{out}}/M_\odot \text{ yr}^{-1} \text{ km s}^{-1}) = 10^{-2.5 \pm 0.3} (S_\nu d^2 / \text{mJy kpc}^2)^{1.1 \pm 0.2}$. Wagner et al. (2015) measured a mass accretion rate onto the star HD 169142 of $\dot{M}_{\text{acc}} \simeq (1.5\text{--}2.7) \times 10^{-9} M_\odot \text{ yr}^{-1}$. Assuming a ratio between mass loss rate in jets and mass accretion rate $\dot{M}_{\text{out}}/\dot{M}_{\text{acc}} \simeq 0.1$ (Cabrit 2007), we estimate that the outflow momentum rate should be $\dot{P}_{\text{out}} \simeq 10^{-7} M_\odot \text{ yr}^{-1} \text{ km s}^{-1}$. Therefore, the correlation would predict a flux density at 3 cm $S_\nu \simeq 5 \mu\text{Jy}$, which is lower than our estimated flux density of $20 \pm 5 \mu\text{Jy}$ for the central radio source. Even though this estimate has large uncertainties, it suggests that an additional mechanism other than shocks associated with the outflow could contribute to the ionization of this jet.

Another possibility is that the observed central radio source was originated as a result of photoionization by high energy radiation from the central star. Extreme-UV (EUV) and, to a lesser extent, X-rays radiation impinging on the inner disk can ionize its surface (Clarke et al. 2001; Gorti et al. 2009; Owen et al. 2010) and contribute to the observed free-free emission. An inhomogeneous inner disk could lead to an inhomogeneous irradiation of its surface, which could result in the asymmetric morphology of the central radio source observed at 7 mm. Additionally, the ejected gas in the accretion-driven jet could also be significantly photoionized by the high-energy radiation emitted by the star (Hollenbach & Gorti 2009).

Finally, the peak of emission of the central radio source could be tracing the position of an independent object at a radius of ~ 3 au from the central star. Given the proximity to the central star, the dynamical timescales involved would be short. An orbiting object at a radius of $\lesssim 3$ au would have an orbital period $\lesssim 4$ yr, and would show detectable orbital proper motions in a few months. On the other hand, knots of emission in a radio jet are expected to be ejected with velocities of $\sim 300 \text{ km s}^{-1}$. Given the small inclination angle of the disk ($i = 13^\circ$, Raman et al. 2006), after projection on the plane-of-the-sky, this would result in proper motions of $\sim 0''.12 \text{ yr}^{-1}$ away from the central star along $PA \simeq -80^\circ$. Future observations should reveal detectable variations and/or proper motions in the observed emission that will allow us to discriminate whether it traces material ejected from the central star (jet) or orbiting

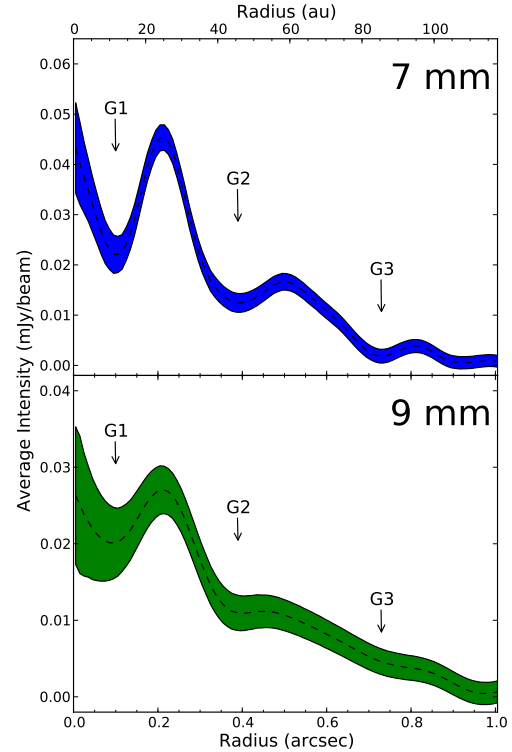


Figure 4. Averaged radial intensity profiles of the 7 mm (top panel) and 9 mm (bottom panel) images. The width of the lines indicates the 1σ uncertainty.

around it (disk or independent object).

3.3. Outer gaps

In order to improve the signal to noise ratio of the detected intensity, we have obtained the averaged radial intensity profiles of the 7 and 9 mm images (see Fig. 4). These profiles were produced by averaging the intensity within concentric elliptical rings, matching the inclination and position angle of the disk major axis determined by previous molecular line observations ($i = 13^\circ$, and $PA = 5^\circ$; Raman et al. 2006). The width of the concentric rings was set to the size of the beam, since the rms noise at spatial scales smaller than a beam is not independent.

Besides the inner gap (hereafter G1), two other gaps at radii $\sim 0.38''$ (~ 45 au; G2) and $\sim 0.73''$ (~ 85 au; G3) are revealed at both 7 mm and 9 mm. The inner (G1) and second gaps (G2) were already detected at near-IR wavelengths (with G1 at radii $\lesssim 0''.19$ and G2 extending from $\sim 0''.28$ to $\sim 0''.48$; Quanz et al. 2013; Momose et al. 2015), at 7 mm (Osorio et al. 2014), and at 1.3 mm (Fedele et al. 2017). Our observations detect the G1 and G2 gaps at the same radii than precedent studies, while the G3 gap is reported here for the first time.

We point out that a sharp cutoff in the uv coverage of the observations can result in the creation of a spurious annular structure during the deconvolution process. However, this artifact would appear at different radii in the images at different frequencies, whereas the G3 gap appears at the same radius in our observations at 7 and 9 mm. Additionally, our simulated images (see §3.1) do not show the presence of spurious features mimicking the G3 gap when an actual gap is not included in the model. Therefore, we conclude that the G3 gap is probably a real annular gap in the disk of HD 169142. We note, however, that the G3 gap is not visible in the ALMA 1.3 mm images (Fedele et al. 2017). This could indicate that the G3 gap is more prominent in the distribution of the cm-sized dust grains traced by our VLA observations.

As mentioned above, different studies have proposed that G1 and G2 are probably formed because of dynamical interactions between the disk and forming planets within each gap (Reggiani et al. 2014; Osorio et al. 2014; Momose et al. 2015; Wagner et al. 2015; Fedele et al. 2017). However, the origin of the third gap (G3) is more difficult to understand. Detection of gaps at such large distances, like G3, is very difficult. So far, similar gaps have only been detected in the protoplanetary disks around HL Tau (ALMA Partnership et al. 2015), TW Hya (Andrews et al. 2016), and HD 163296 (Isella et al. 2016), through recent extremely high angular resolution ALMA observations. The density in the disk mid-plane at such large distances is probably too low to create a planet responsible for clearing the observed gap. Alternatively, the magneto-rotational instability (MRI) in magnetized disks can produce pressure bumps at the outer edges of the dead zones in the disk, which can in turn trap the large dust grains and create gaps in the mm emission of the disk (Flock et al. 2015). However, dead zones are expected to be closer to the central star (at radii ~ 50 au), so models do not predict gaps as far as the observed G3 gap in HD 169142.

Another possible origin for G3 would be grain growth and/or an increase in the solids surface density close to condensation fronts (i.e. snowlines) of volatiles in the disk. This process has been suggested as the responsible for some of the rings and gaps that were detected by ALMA in the disk around the younger T Tauri star HL Tau (ALMA Partnership et al. 2015; Zhang et al. 2015; Okuzumi et al. 2016). Models and laboratory experiments suggest that dust grains can grow significantly when surrounded by an icy mantle, which would form on the surface of the grains beyond these snowlines (Ros & Johansen 2013; Testi et al. 2014 and references therein). In addition, it has been suggested that the enhanced surface density of solids beyond the snowline can produce viscosity gradients and pressure bumps because

of a reduction in the column depth of the MRI-active layer. These pressure bumps could in turn trap the large dust grains (Kretke & Lin 2007), although more recent studies have found that, at least for the water snowline, which is located at much smaller radii, the viscosity gradient would need to be unrealistically high to be able to form a dust trap (Bitsch et al. 2014).

Based on the composition of comets, the most abundant volatiles in protoplanetary disks are thought to be water, CO, and CO₂. These molecules have, for typical disk mid-plane densities, condensation temperatures of 128–155 K, 23–28 K, and 60–72 K, respectively (Zhang et al. 2015). Comparing these temperatures with the mid-plane temperatures obtained from the model presented by Osorio et al. (2014), we find that the water and CO₂ snowlines would fall inside G1, while the CO snowline would be located at a distance of 90–130 au³. The lower end of the range of radii for the CO snowline is coincident with the outer edge of G3, favoring grain growth and an increase in the solids surface density close to the CO snowline as a possible mechanism to explain the origin of the G3 gap.

An independent measurement of the position of the CO snowline in protoplanetary disks can be obtained through observations of molecules whose chemistry is sensitive to the CO (Qi et al. 2013). One of these molecules is the DCO⁺, which is expected to form mainly in the regions of protoplanetary disks where gas-phase CO and low temperatures ($T < 30$ K) coexist. Because of this, the DCO⁺ emission has been used as a tracer of the CO freeze-out in disks, showing a ring-like morphology peaking at just a slightly smaller radius than the CO snowline (Mathews et al. 2013; Öberg et al. 2015). However, recent studies suggest that, in some cases, the DCO⁺ molecule might have a more complex relationship with the CO snowline, and that optically thin CO isotopologues such as C¹⁸O could represent better tracers by showing a decrease of emission at the radius of the snowline (Qi et al. 2015; Huang et al. 2017).

In order to estimate the position of the CO snowline in HD 169142, we have analyzed ALMA archival observations of both the DCO⁺(3-2) and C¹⁸O(2-1) molecular transitions. An image of the velocity-integrated DCO⁺(3-2) emission is shown in Fig. 5, whereas the C¹⁸O(2-1) images are reported by Fedele et al. (2017). We have obtained averaged radial profiles of the velocity-integrated emission for both transitions following the same procedures as for the continuum emission

³ We note that the Osorio et al. (2014) model used a distance of 145 pc, which is a $\sim 20\%$ larger than the recent distance of 117 pc measured by Gaia. However, we do not expect important changes in the physical structure of the disk.

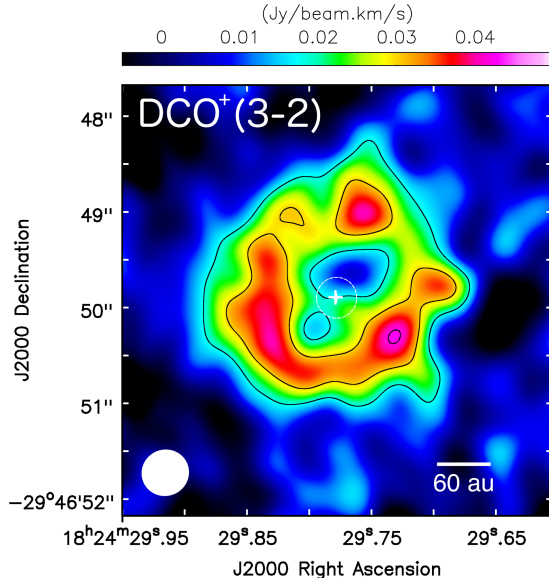


Figure 5. Velocity-integrated intensity (zero-order moment) of the $\text{DCO}^+(3-2)$ emission of the disk around HD 169142 (synthesized beam= $0''.50 \times 0''.48$, PA= -65° ; shown in the lower-left corner). Contour levels are $-3, 3, 5, 7$, and 9 times the rms of the map, $6.0 \mu\text{Jy beam}^{-1} \text{ km s}^{-1}$. The dashed ellipse indicates our fit to the ring image at 7 mm (Fig. 1). The white cross shows the position of the star.

(see Fig. 6). The image of the $\text{DCO}^+(3-2)$ emission shows a ring morphology (Fig. 5) with radius $\sim 0''.80$ ($\sim 95 \text{ au}$), as it is clearly seen in the radial profile shown in Fig. 6. Additionally, the $\text{C}^{18}\text{O}(2-1)$ emission shows a significant change of slope in its radial profile at $\sim 0''.85$ ($\sim 100 \text{ au}$), indicating a decrease of the gas-phase CO beyond this radius. Thus, both molecular transitions indicate that the CO snowline is located at $\sim 100 \text{ au}$ in the disk of HD 169142, very close to the G3 gap and in the range of distances estimated with the Osorio et al. (2014) model.

These results suggest that the G3 gap might be produced because of an accumulation of large dust grains at the position of the CO snowline. Large grains could grow and accumulate close to the CO snowline, creating a ring of emission at long wavelengths next to an inner zone with a lower density of large grains, resulting in the observed gap in the 7 mm emission of the disk. As noted above, the 1.3 mm emission of the disk does not show the presence of G3 gap (Fedele et al. 2017), which could indicate that the larger ($\sim \text{cm}$ -sized) dust grains are being trapped in the CO snowline (Kretke & Lin 2007), whereas the smaller ($\sim \text{submm/mm}$ -sized) grains traced by the 1.3 mm emission have continued their inward migration. Further studies, including both modeling and observations, are needed to fully understand the possible changes in the disk appearance with the observing wavelength.

Therefore, even though we cannot completely discard

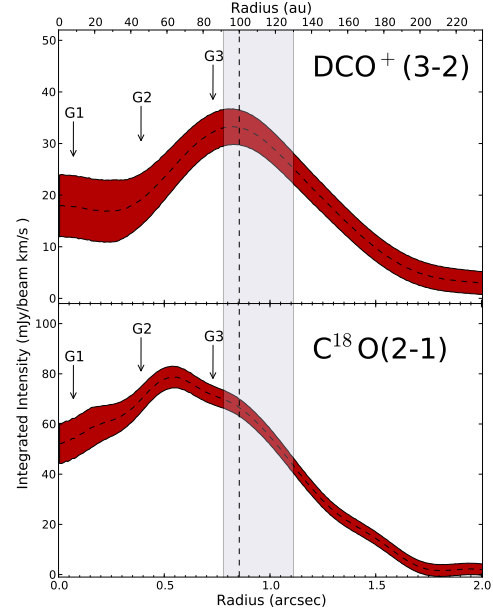


Figure 6. Radial profiles of the averaged velocity-integrated intensity (zero-order moment) of the $\text{DCO}^+(3-2)$ (top panel) and $\text{C}^{18}\text{O}(2-1)$ emission (lower panel). The width of the lines indicates the 1σ uncertainty. The G1, G2, and G3 labels indicate the position of the three gaps detected at 7 and 9 mm . The shaded region between 90 and 130 au indicates the range of distances for the CO snowline estimated from the Osorio et al. (2014) model. The vertical dashed line indicates the proposed position of the CO snowline based on the change in slope of the $\text{C}^{18}\text{O}(2-1)$ emission and the position of the $\text{DCO}^+(3-2)$ ring.

a magnetically induced or planet-induced origin, we favor dust growth and accumulation of large dust grains close to the CO snowline as the most likely mechanism responsible for the proposed G3 gap in HD 169142.

4. SUMMARY AND CONCLUSIONS

We have presented new high angular resolution VLA observations at 7 mm , 9 mm , and 3 cm toward the pre-transitional disk around HD 169142. Our main results can be summarized as follows:

- Our 7 and 9 mm observations show a narrow ($\sim 8 \text{ au}$ in width) azimuthally asymmetric ring of emission of radius $\sim 25 \text{ au}$, apparently tracing the outer rim of the innermost gap. The radius of the ring is consistent with that of previous 7 mm and near-IR polarized scattered light images (Quanz et al. 2013; Osorio et al. 2014; Momose et al. 2015). A bright knot of emission in the ring is revealed at 7 mm . This knot of emission is not present in the near-IR images, indicating that it is probably tracing an azimuthal asymmetry in the density of the disk mid-plane, to which our 7 mm images are

more sensitive. We interpret this asymmetry as probably produced by tidal interactions between the disk and forming planets.

- A central component of emission is detected inside the inner gap at 7 mm, 9 mm, and 3 cm. The 7 mm source shows a slightly elongated morphology approximately along the E-W direction, with its peak of emission displaced a projected distance of ~ 3 au ($\sim 0''.025$) to the west of the central star. The flux density and spectral index of this central radio source indicate that it is dominated by free-free emission from ionized gas, which could be associated with an inhomogeneous photoionization of the inner disk, with an independent orbiting object, or with an (asymmetric) ionized jet. Although data currently available seem to favor the latter scenario, future observations should reveal significant proper motions either away or around the central star that will allow us to discriminate between ejection or orbital motions.
- The radial intensity profiles of the 7 and 9 mm images reveal the presence of multiple gaps in the disk of HD 169142. Our 7 and 9 mm observations not only confirm the presence of the previously reported inner (G1) and second (G2) gaps, which approximately extend through radii ~ 0 –25 au and ~ 32 –56 au, respectively, but also detect, for the first time, a new gap comprising the radii ~ 77 –96 au (G3). This proposed gap, one of the farthest gaps ever detected in a protoplanetary disk, is not detected in ALMA 1.3 mm images, suggesting that it might be more prominent in the distribution of

the larger dust grains traced by our VLA observations.

- Our analysis of $\text{DCO}^+(3-2)$ and $\text{C}^{18}\text{O}(2-1)$ ALMA observations, as well as the results of the [Osorio et al. \(2014\)](#) model, indicate that the CO snowline is located at ~ 100 au. This suggests that dust grain growth and an increase in the solids surface density close to the CO snowline could be the mechanism responsible for the origin of the proposed G3 outer gap.

We thank an anonymous referee for useful and valuable comments. This paper makes use of the following ALMA data: ADS/JAO.ALMA#2013.1.00592.S. ALMA is a partnership of ESO (representing its member states), NSF (USA) and NINS (Japan), together with NRC (Canada), NSC and ASIAA (Taiwan), and KASI (Republic of Korea), in cooperation with the Republic of Chile. The Joint ALMA Observatory is operated by ESO, AUI/NRAO and NAOJ. E.M., G.A., M.O., J.M.T., and J.F.G. acknowledge support from MINECO (Spain) grant AYA2014-57369-C3 (co-funded with FEDER funds). JMT acknowledges support from the Generalitat de Catalunya/CERCA programme. C.C.-G. acknowledges support from UNAM-DGAPA PAPIIT IA102816.

Facilities: VLA

Software: CASA (v 4.3.1, 4.5.3; [McMullin et al. 2007](#))

REFERENCES

- Alexander, R., Pascucci, I., Andrews, S., Armitage, P., & Cieza, L. 2014, in *Protostars and Planets VI*, ed. H. Beuther et al. (Tucson, AZ: Univ. Arizona Press), 475
- ALMA Partnership, Brogan, C. L., Pérez, L. M., et al. 2015, *ApJL*, 808, L3
- Andrews, S. M., Wilner, D. J., Espaillat, C., et al. 2011, *ApJ*, 732, 42
- Andrews, S. M., Wilner, D. J., Zhu, Z., et al. 2016, *ApJL*, 820, L40
- Anglada, G. 1995, *RMxAC*, 1, 67
- Anglada, G., Rodríguez, L. F., & Carrasco-González, C. 2015, in *Advancing Astrophysics with the Square Kilometre Array (AASKA14)*, 121
- Bai, X.-N., & Stone, J. M. 2014, *ApJ*, 796, 31
- Baruteau, C., Crida, A., Paardekooper, S.-J., et al. 2014, in *Protostars and Planets VI*, ed. H. Beuther et al. (Tucson, AZ: Univ. Arizona Press), 667
- Billar, B. A., Males, J., Rodigas, T., et al. 2014, *ApJL*, 792, L22
- Birnstiel, T., Dullemond, C. P., & Pinilla, P. 2013, *A&A*, 550, L8
- Bitsch, B., Morbidelli, A., Lega, E., Kretke, K., & Crida, A. 2014, *A&A*, 570, A75
- Blondel, P. F. C., Djie, H. R. E. T. A. 2006, *A&A*, 456, 1045
- Cabrit, S. 2007, in *IAU Symp. 243, Star-Disk Interaction in Young Stars*, ed. J. Bouvier & I. Appenzeller (Cambridge: Cambridge Univ. Press), 203
- Calvet, N., D'Alessio, P., Watson, D. M., et al. 2005, *ApJ*, 630, L185
- Clarke, C. J., Gendrin, A., & Sotomayor, M. 2001, *MNRAS*, 328, 485
- Dent, W. R. F., Torrelles, J. M., Osorio, M., Calvet, N., & Anglada, G. 2006, *MNRAS*, 365, 1283
- Ercolano, B., Rosotti, G. P., Picogna, G., & Testi, L. 2017, *MNRAS*, 464, L95
- Espaillat, C., Calvet, N., D'Alessio, P., et al. 2007, *ApJL*, 670, L135
- Espaillat, C., Muzerolle, J., Najita, J., et al. 2014, in *Protostars and Planets VI*, ed. H. Beuther et al. (Tucson, AZ: Univ. Arizona Press), 497
- Fedele, D., Carney, M., Hogerheijde, M. R., et al. 2017, *arXiv:1702.02844*
- Flock, M., Ruge, J. P., Dzyurkevich, N., et al. 2015, *A&A*, 574, A68
- Gaia Collaboration, Brown, A. G. A., Vallenari, A., et al. 2016, *arXiv:160904172*

- Gorti, U., Dullemond, C. P., & Hollenbach, D. 2009, *ApJ*, 705, 1237
- Grady, C. A., Schneider, G., Hamaguchi, K., et al. 2007, *ApJ*, 665, 1391
- Guidi, G., Tazzari, M., Testi, L., et al. 2016, *A&A*, 588, A112
- Hollenbach, D., Gorti, U. 2009. *ApJ*, 703, 1203
- Honda, M., Maaskant, K., Okamoto, Y. K., et al. 2012. *ApJ*, 752, 143
- Huang, J., Öberg, K. I., Qi, C., et al. 2017, *ApJ*, 835, 231
- Isella, A., Chandler, C., Carpenter, J. M., Pérez, L. .M., Ricci, L. 2014, *ApJ*, 788, 129
- Isella, A., Guidi, G., Testi, L., et al. 2016, *PhRvL*, 117, 251, 101
- Kretke, K. A., & Lin, D. N. C. 2007, *ApJ*, 664, L55
- Maaskant, K. M., Honda, M., Waters, L. B. F. M., et al. 2013, *A&A*, 555, A64
- Macías, E., Anglada, G., Osorio, M., et al. 2016, *ApJ*, 829, 1
- Manoj, P., Bhatt, H. C., Maheswar, G., & Muneer, S. 2006, *ApJ*, 653, 657
- Mathews, G. S., Klaassen, P. D., Juhás, A., et al. 2013, *A&A*, 557, A132
- McMullin, J. P., Waters, B., Schiebel, D., Young, W., & Golap, K. 2007, *Astronomical Data Analysis Software and Systems XVI* (ASP Conf. Ser. 376), ed. R. A. Shaw, F. Hill, & D. J. Bell (San Francisco, CA: ASP), 127
- Meeus, G., Pinte, C., Woitke, P., et al. 2010, *A&A*, 518, L124
- Momose, M., Morita, A., Fukagawa, M., et al. 2015, *PASJ*, 67, 83
- Monnier, J. D., Harries, T. J., Aarnio, A., et al. 2017, [arXiv:1702.04780](https://arxiv.org/abs/1702.04780)
- Öberg, K. I., Furuya, K., Loomis, R., et al. 2015, *ApJ*, 810, 112
- Okuzumi, S., Momose, M., Sirono, S., Kobayashi, H., & Tanaka, H. 2016, *ApJ*, 821, 82
- Osorio, M., Anglada, G., Carrasco-González, C., et al. 2014, *ApJL*, 791, L36
- Osorio, M., Macías, E., Anglada, G., et al. 2016, *ApJL*, 825, L10
- Owen, J. E., Ercolano, B., Clarke, C. J., & Alexander, R. D. 2010, *MNRAS*, 401, 1415
- Owen, J. E., Scaife, A. M. M., Ercolano, B. 2013, *MNRAS*, 434, 3378
- Qi, C., Öberg, K. I., Andrews, S. M., et al. 2015, *ApJ*, 813, 128
- Qi, C., Öberg, K. I., Wilner, D. J., et al. 2013, *Science*, 341, 630
- Quanz, S. P., Avenhaus, H., Buenzli, E., et al. 2013, *ApJL*, 766, L2
- Quanz, S. P., Schmid, H. M., Geissler, K., et al. 2011, *ApJ*, 738, 23
- Raman, A., Lisanti, M., Wilner, D. J., et al. 2006, *AJ*, 131, 2290
- Rau, U., Cornwell, T. J. 2011, *A&A*, 532, 71
- Reggiani, M., Quanz, S. P., Meyer, M. R., et al. 2014, *ApJL*, 792, L23
- Reid, M. J., Schneps, M. H., Moran, J. M., et al. 1988, *ApJ*, 330, 809
- Rodríguez, L. F., Zapata, L. A., Dzib, S. A., et al. 2014, *ApJL*, 793, L21
- Ros, K., & Johansen, A. 2013, *A&A*, 552, A137
- Seok, J. Y., & Li, A. 2016, *ApJ*, 818, 2
- Strom, K. M., Strom, S. E., Edwards, S., Cabrit, S., & Skrutskie, M. F. 1989, *AJ*, 97, 1451
- Testi, L., Birnstiel, T., Ricci, L., et al. 2014, in *Protostars and Planets VI*, ed. H. Beuther et al. (Tucson, AZ: Univ. Arizona Press), 339
- van Boekel, R., Min, M., Waters, L. B. F. M., et al. 2005, *A&A*, 437, 189
- Wagner, K. R., Sitko, M. L., Grady, C. A., et al. 2015, *ApJ*, 798, 94
- Zhang, K., Blake, G. A., & Bergin, E. A. 2015, *ApJL*, 806, L7
- Zhu, Z., & Stone, J. M. 2014, *ApJ*, 795, 53